

Modelling infrared signatures of ships and decoys for countermeasure effectiveness studies

Ric (H.)M.A. Schleijsen*, Marianne A.C. Degache, Henny E.T. Veerman,
Ronald van Sweeden, Bernadetta A. Devecchi.
TNO Defence, Security and Safety, P.O. Box 96864
2509 JG The Hague, The Netherlands

ABSTRACT

Infrared guided missiles are a threat for modern naval forces. The vulnerability of ships can be reduced by applying countermeasures such as infrared decoys and infrared signature reduction.

This paper presents recent improvements in a simulation toolset which can be used for assessing the effectiveness of these measures. The toolset consists of a chain of models, which calculate the infrared signature of a ship (EOSM) and decoys, and generate infrared image sequences of the ship in a realistic sea and sky background (EOSTAR). A complete missile fly-out model (EWM) uses these images in closed loop simulations for the evaluation of countermeasure effectiveness against simulated seekers. All model components will be discussed. Typical simulation results will be shown.

Keywords: Infrared signatures, Infrared countermeasures, Anti Ship Missile Defence

1. INTRODUCTION

The ability of a navy ship to perform its tasks in conflict situations determines the operational effectiveness of this platform. The survivability is an important component of the operational effectiveness. Here we narrow down to one particular aspect of the survivability: the susceptibility. The susceptibility of a platform is determined by the processes starting with the probability of detection of a platform up to the probability that the platform eventually will be hit by an enemy weapon. This paper focuses on the susceptibility of a navy ship in relation to infrared guided threats.

Against infrared guided anti ship missiles, the combination of infrared ship signature reduction and the deployment of infrared decoys can be very effective in hit avoidance. Various techniques for signature reduction have been developed over time. For example studies on the effect of exhaust gas cooling by either mixing cool air or water with the exhaust gases have been reported in reference 1 and 2 respectively. Cooling of the hull and parts of the superstructure with cold water from the pre-wetting installation on board of the ship is another way of reducing the signature, which has been presented in reference 3. Infrared decoys can be used to interrupt the guidance from a missile towards the ship. The timing and the direction of the decoy launches is very critical for the success and many studies have been dealing with this issue, as for example reported in references 4 and 5.

References 6 and 7 report on the development of a "toolset for evaluating infrared countermeasures and signature reduction for ships". A schematic overview of this toolset is shown in figure 1. The extension of this toolset with a detailed decoy model is the main topic of this paper. The common part in the toolset is the engagement part of the model. This part is based on the Electronic Warfare Model (EWM). EWM is a system that is capable of performing closed-loop simulations regarding the engagement of missiles against ships. It is a TNO in-house development which was originally designed for simulation of electronic countermeasure effectiveness in radar guided missile engagements. EWM now includes detailed seeker models both for infrared and radar guided missiles. These seeker models simulate the details of the interaction of the seeker with targets and decoys. The missile flight dynamics are also simulated in a detailed manner, including a 6 degree of freedom missile fly-out model. The targets can be represented in different levels of detail, depending on the requirements in the study. A more detailed description of EWM is given in reference 8.

* ric.schleijsen@tno.nl, phone +31 888 66 3837, fax +31 888 666 575, www.tno.nl

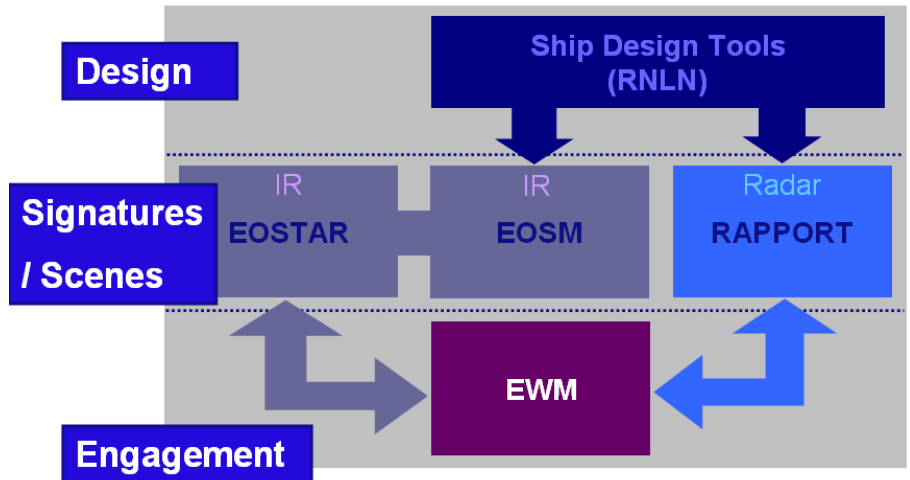


Figure 1: Relation between the components EOSTAR, EOSM and EWM of the TNO toolset

The EW model has been used to develop decoy countermeasure deployment strategies, including combinations of decoys and jamming. These deployment strategies have been implemented in a Tactical Decision Aid (TDA) for optimum countermeasure deployment, currently in use on board of platforms of the Royal Netherlands Navy. The TDA calculates the optimum timing of the decoy launches and provides advice on ship manoeuvres in order to generate the maximum miss distance. A derivative of this TDA is implemented in the EW model in order to optimise the decoy deployment in the simulations automatically. Alternatively the decoy deployment can be programmed manually for the simulations.

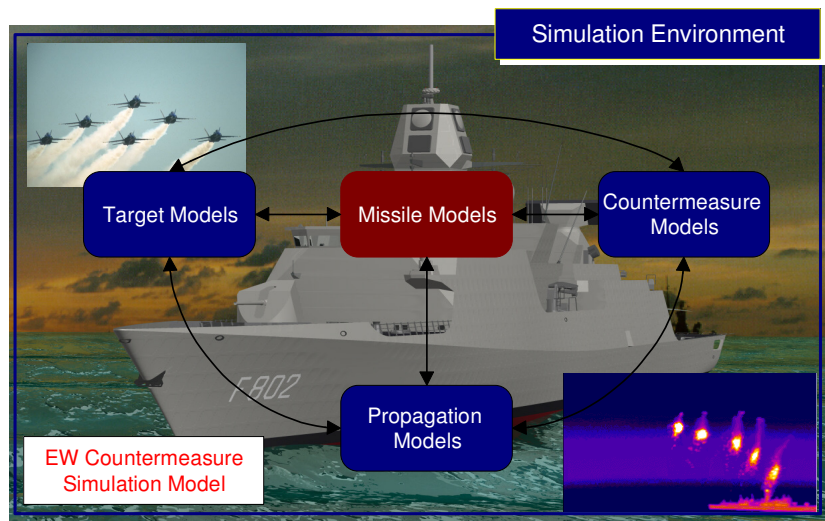


Figure 2: Schematic overview of the TNO Electronic Warfare Model

The model simulates the decoy deployment, for both RF (Chaff) and Infrared decoys. This includes the timing of the decoy launches, the calculation of the position where the decoys bloom and the subsequent drift of the decoys by the wind. Since the decoy effectiveness depends to a large extent on the location of the decoys with respect to the ship (horizontal distance and altitude), this is a critical factor in the simulations. Reference 7 indicates that for studies of decoy effectiveness against imaging seekers the level of detail in the modelling of decoys and ships has to match the resolution of the imaging seeker when the decision on the decoy rejection has to be made by the seeker. In reference 7

the steps towards increased resolution in ship modelling have been shown. The infrared signature modelling is based on the EOSM component of the EOSTAR model suite (reference 9) and the validation of the EOSM signature part of this model has been reported in reference 10.

The increase of the level of detail in the infrared decoy in simulated images, based on models of the physics behind and the application of these images in countermeasure effectiveness studies is the main topic of this paper.

This paper is organised as follows: Section 2 reports on actual data collection on a ship launching decoys for model development and validation. In Section 3 the physics based decoy modelling is presented. Section 4 presents the results of the actual implementation of the IR decoy model. Section 5 discusses the use of the model suite to generate sequences of synthetic scenes with a ship deploying decoys for decoy effectiveness studies. Section 6 illustrates the option for generating scene sequences of a ship applying active signature management. Summarised findings and conclusive remarks are given in Section 7.

2. DATA COLLECTION IN SUPPORT OF MODELLING

In September 2011 the NATO RTO study group SET-144 conducted the SQUIRREL trial as a part of the RIMPASSE trial sequence organised by the German-Netherlands Centre for Ship Signature Management (CSSM) together with a number of NATO study groups. The main focus of the SQUIRREL trial in northern Germany was on infrared ship signature management. For this purpose the Canadian research vessel Quest was equipped with an active hull cooling system in order to match the hull temperature to the apparent temperature of the local environment and a sea water injection system to cool down the exhaust gases in order to reduce the infrared emission of the plume. In conjunction with the signature management infrared decoys were launched. The effects of the signature management on the infrared signatures and the decoy signatures were measured and analysed quantitatively. The results are classified. However, we will show some un-calibrated imagery from the trial to illustrate the use of the trial data for model validation.

Typical decoy runs were performed at a range of several km. One or more decoys were launched during several runs of the ship in different configurations of the signature management systems. We recorded these events and the recorded imagery was used to test the Imaging Infrared Seeker model as currently implemented in the EWM model. For this purpose the closed loop simulation image input from EOSTAR/EOSM into the seeker model is now replaced by the recorded imagery. Some scenes from the resulting seeker output are shown in figure 3.

The design of the imaging seeker is inspired by a linear array detector, scanning the horizon. For target detection a threshold level is derived for each line of the image based on the noise level in this line near the edges of the image. The areas of the image with grey levels above the threshold are marked as potential target areas. Negative contrasts can be tracked as well. The target areas from the different lines above the threshold are combined to one target area. In the acquisition phase the seeker scans the horizon from left to right and vice versa. When the target is detected in two subsequent scans a track-box is defined around the target, leaving a small margin around the target. The centre of the track-box is taken to derive the tracking point. During the tracking phase, only the potential target areas within the track-box are evaluated. The size of the track-box increases when the size of the target area increases. This is done to accommodate the apparent growth in size of the ship target while the missile approaches the ship, but the track box also increases in size when a decoy enters the tracking box. In case there are two potential targets in the track box, the seeker selects the largest target as the true target. Additional counter-counter measures such as comparing the average grey level of the target and the decoys are not implemented yet.

In the first image (a) in figure 3 the seeker tracks the whole ship. Due to the low infrared emission between the bow and the main part of the ship in the second image (b), the seeker interprets the ship as two separated targets and selects the largest one. This can be an important check for the robustness of the seeker tracking on real imagery, because in the simulations such a split of the target never appears. In some seeker runs on other recorded sequences with more noise, the seeker selects the bow of the ship as the most attractive target. In the third image (c) the small flash of the decoy launch from below the bridge can be observed. In the fourth image (d) the decoy has just bloomed. Decoy and ship overlap and the seeker considers them as one target. In the fifth image (e) the decoy reaches its maximum size. The sixth image (f) is the image just before the moment where the decoy and ship separate and where the seeker has to take the decision on which potential target to follow. The seventh image (g) shows that the seeker has selected the ship as the target. Despite the higher emission of the decoy the seeker has decided for the larger target area of the ship.

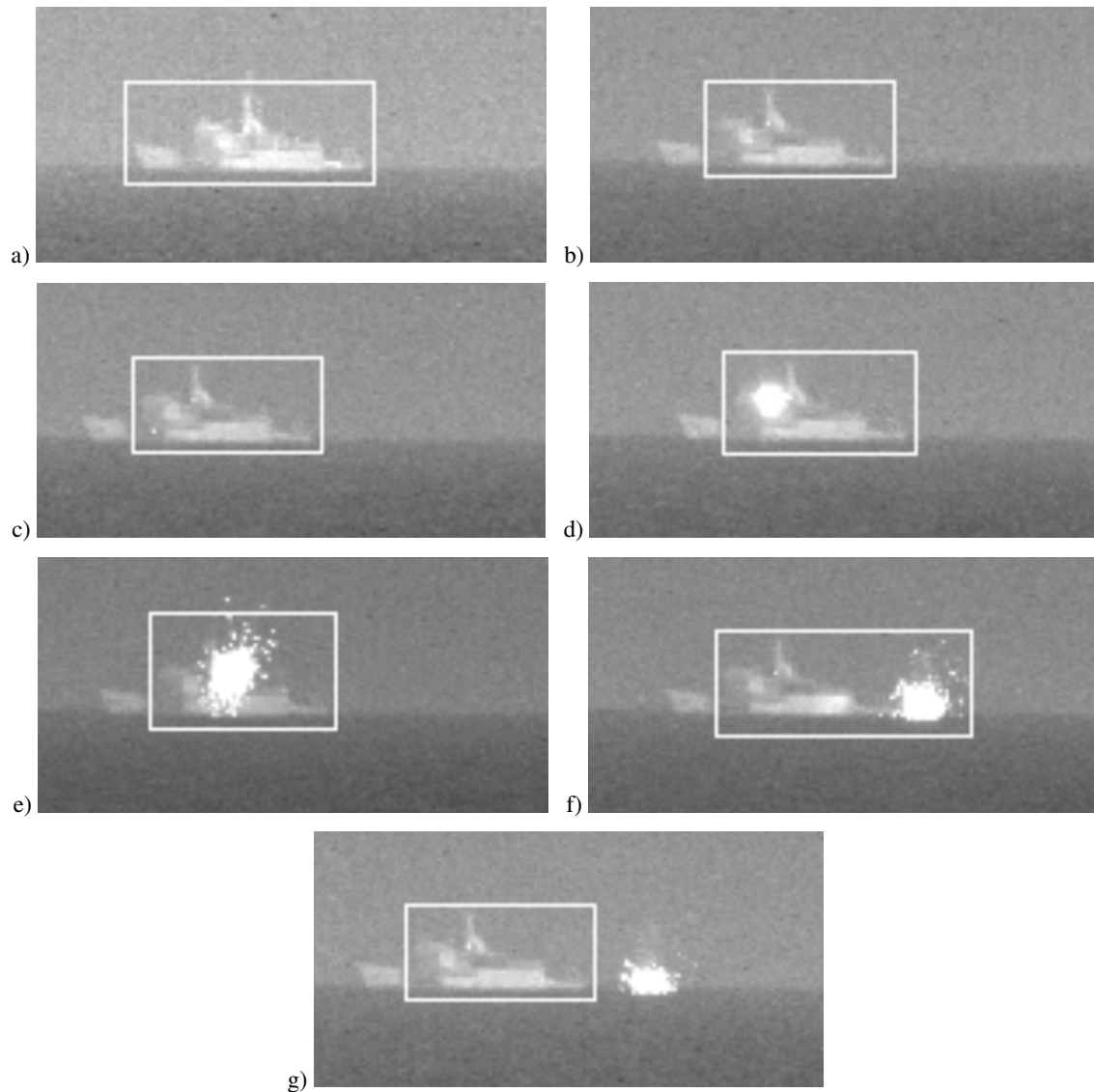


Figure 3: Scenes EWM imaging seeker output on recorded imagery.

Image sequences of these decoy launches combined with some close up imagery of the decoys at short range have been used in support of infrared decoy modelling in the EOSTAR/EOSM model. From the imagery a number of observables from the decoys were extracted by analysing the grey levels of the images. The first and second observables are the apparent size of the decoy blob in number of pixels (the effective area A_{eff}) and the total intensity of the decoy in bits (summed intensity ΣI) respectively. The maximum intensity level (I_{max}) in the decoy area shows a peak when the decoy starts to bloom, due to the explosion of the round which initiates the burn and the dispersal of the burning particles. Apart from the initial peak the mean intensity ($\langle I \rangle$) of the decoy remains more or less constant. This indicates that the small particles burn at a more or less constant level over time. This mean intensity at a more or less constant level also leads to a strong similarity in shape of the curves for the number of pixels and the total intensity. The standard deviation of the decoy intensity is another parameter to be taken into account in the decoy model. Finally the trajectory of the decoy needs to be analysed and modelled. Graphs for these observables as a function of time are presented in figure 4. Figure 5 shows a visible band image of a decoy launch.

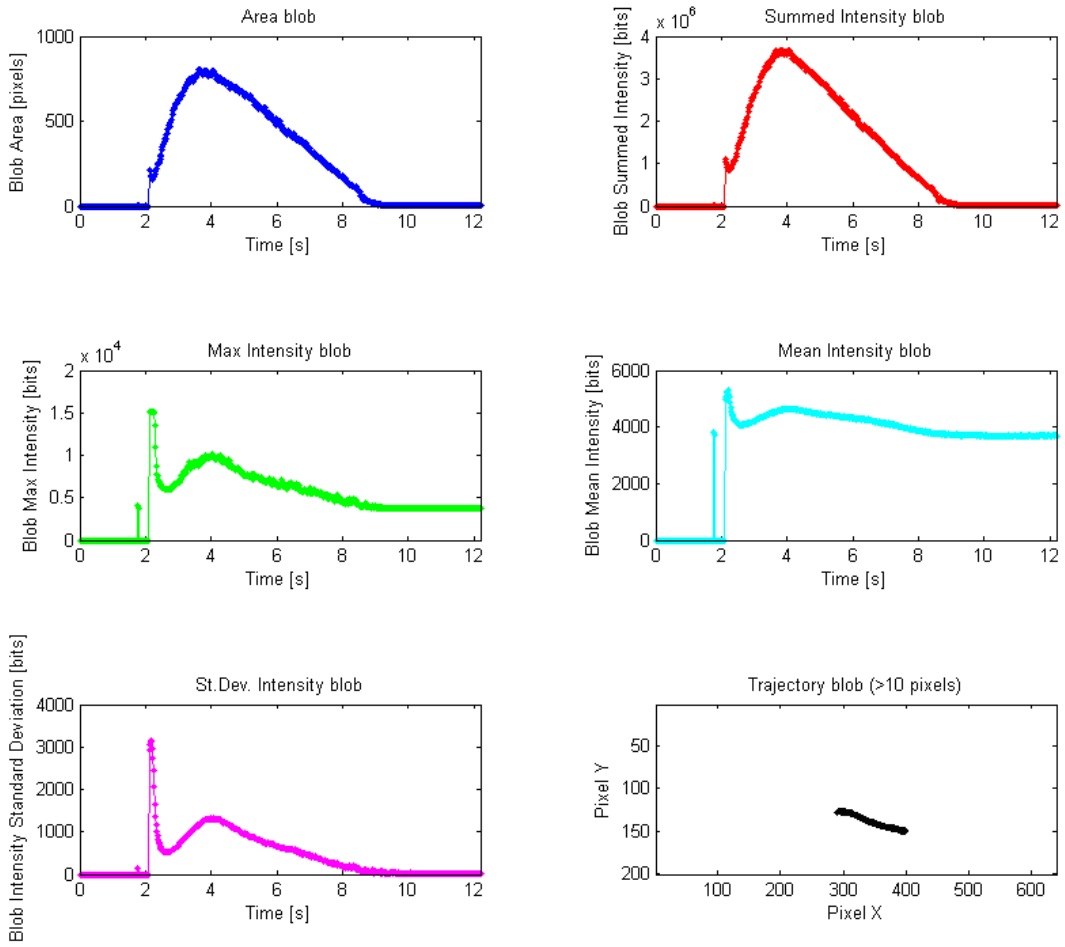


Figure 4: Observables in decoy image sequences: from left to right and top to bottom: the apparent size of the decoy blob in number of pixels, the total intensity of the decoy in bits, the maximum intensity level in the decoy, the mean intensity of the decoy, the standard deviation of the decoy intensity and the decoy trajectory.



Figure 5: Visible band image of the ship launching a decoy.

3. INFRARED DECOY MODELLING

The representation of the flares in the infrared scene is based on physical modelling of the flare behaviour, resulting in flare models which result in the same behaviour of the flare observables as extracted from the measurements. The evolution of the flare is described as consisting of two different phases.

The first phase refers to the period from launch to ignition. The trajectory of the flare is found solving a set of equations that describe the evolution of its centre of mass position and velocity. The dynamical evolution is dictated by the acceleration \mathbf{a} :

$$\mathbf{a} = \mathbf{g} + \mathbf{a}_{drag}$$

Where \mathbf{g} is the gravitational acceleration and \mathbf{a}_{drag} is a correction term that takes into account the drag caused by the wind. \mathbf{a}_{drag} is directed opposite to the relative velocity between the flare and the air, its module being $\frac{1}{2}\rho v^2 C_D A/m$, with A and m the effective area and mass of the decoy respectively, v the decoy relative velocity with respect to air, C_D the drag coefficient and ρ the air density.

Phase two starts with the explosion of the decoy, which is described in a way similar to what is done in firework models (see for example reference 11). After the explosion the burning material starts chemical reactions that release energy. This has the effect of releasing the gas and solid particles responsible for the IR emission of the flare. The expansion of the material is driven by the increase in pressure P due to the release of chemical energy. The expansion of the decoy cloud will terminate once P equals the pressure of the ambient air P_{air} . If we assume that the material follows the perfect gas law, a characteristic length scale for the explosion can be determined that is given by:

$$L_f \cong \sqrt{\frac{nR \Delta U}{c_v P_{air}}}$$

Where n is the number of moles per gram produced during the reaction, c_v the specific heat at constant volume, $\Delta U(t)$ the amount of increase of internal energy and R the gas constant.

We assume that gas and solid particles follow the same spatial distribution around their common centre of mass \mathbf{x}_{cm} . The dynamical evolution of the latter is similar as in phase one, but in now the effect of buoyancy is also taken into account, thus adding a term $L_f^3 \rho_{air} / m \cdot \mathbf{g}$ in the equation of motion.

The shape of the cloud changes due to dispersion into the surrounding environment. To describe the distribution of material as a function of time, we adopt the puff model (reference 12). This is a generalisation of the commonly used Gaussian plume model, adapted for non-stationary conditions. In this formulation the concentration of material at position \mathbf{x} is given by:

$$c(\mathbf{x}) = \frac{M}{\sigma_z \cdot \sigma_h^2} \exp\left[-\frac{1}{2}\left(\frac{x_{cm} - x}{\sigma_h}\right)^2\right] \exp\left[-\frac{1}{2}\left(\frac{y_{cm} - y}{\sigma_h}\right)^2\right] \exp\left[-\frac{1}{2}\left(\frac{z_{cm} - z}{\sigma_z}\right)^2\right]$$

Here σ_z and σ_h are the vertical and horizontal standard deviations, containing the information of how the material dispersion proceeds. The system of reference is such that the wind speed is parallel to the x-axis. The evolution of the cloud is described by the time dependence of σ_z and σ_h . In the regime we are interested in, $\sigma_h^2 = \varepsilon t^3$ where ε is the eddy dissipation rate. A similar prescription is adopted for σ_z , but its value is kept constant after reaching $0.3z$. As the observational dataset for dispersion under non-stationary conditions is less extended then for the case of continuous sources, we also implemented a time-dependency following the procedures adopted for the continuous emission. In this case the atmosphere is classified in stability classes, each class characterized by a different evolutionary function (see reference 13 for an extended discussion on this topic).

Once exposed to the oxygen in the atmosphere, the solid particles will commence oxidation and start burning. To take into account for the non-instantaneous nature of the process, we assume each solid particle starts burning at a different initial time. We model the initial time distribution with a law $t^a(t-\tau)^b$, where a and b are parameters describing the rising and fall of the distribution and τ describes its characteristic spread. We here assume that every solid particle behaves like a black body in the IR range, cooling down from an initial temperature T_{burn} .

To compute the resulting radiant intensity we make use of the radiative transfer code DISORT (references 14 and 15). The volume of the decoy is divided into a 3D rectangular grid. The volumes are defined in such a way that each face in the x - z plane at $y = 0$ corresponds to a pixel in the synthetic image. All the volumes that are along the same line of sight are simulated with the same call to DISORT, and independently from the others. The grid resolution has been chosen high enough as to obtain convergence in the resulting intensity values at $y = 0$. Note however, that at the moment we are only interested in the qualitative time behaviour of the intensity and not on the exact normalization. The absolute values will be tuned to the measured observables.

In figure 6 we present the results of simulations, where we fixed the burning parameters in the model (specifically $T_{burn} = 600^\circ\text{C}$, $\tau = 4.5$ s, $a = 2$ and $b = 2$) to find a good representation of the flares in the trial run shown in figure 3. The evolution of the system can be characterized by the time evolution of the effective area A_{eff} , maximum, mean and summed intensities (I_{max} , $\langle I \rangle$ and ΣI , respectively) of the decoy. To calculate these quantities (and in agreement with what has been done on the observational data) we adopted an intensity threshold I_{th} and we took into account of only those pixels in the synthetic image above I_{th} . As we are here interested only in comparing the qualitative behaviour of each curve, y-axes are normalized to the maximum values assumed by each quantity.

The upper left panel corresponds to the effective area A_{eff} of the decoy. The red line is our reference model, while dotted, dashed and solid black lines correspond to increasing values of I_{th} . The lowest intensity threshold is closer to the physical area L_f^2 of the decoy. The continuous expansion we see in the dotted curve is therefore representative of the cloud physical expansion. As we increase the threshold level I_{th} , we start including only the central more strongly emitting regions in the computation of A_{eff} , ignoring the cooler outer part of the decoy. A_{eff} initially increases due to the increasing number of solid particles that start burning. After $\sim \tau$ s, the material has started cooling down significantly and no more new solid particles are produced. The outer parts of the cloud drop below I_{th} , thus leading to the decrease of A_{eff} .

The upper right panel shows the time evolution of ΣI . The characteristic rise and fall timescale of the red curve are in good agreement with the observational data. The lower left and right panel show $\langle I \rangle$ and I_{max} in the synthetic images respectively. Note that $\langle I \rangle$ increases when we strengthen the intensity threshold, as all the less emitting region of the cloud is progressively not taken into account anymore. Also note that the intensity peak at the flare ignition is not represented in the model, because this peak will not influence the response of the seeker as currently implemented in the EWM model.

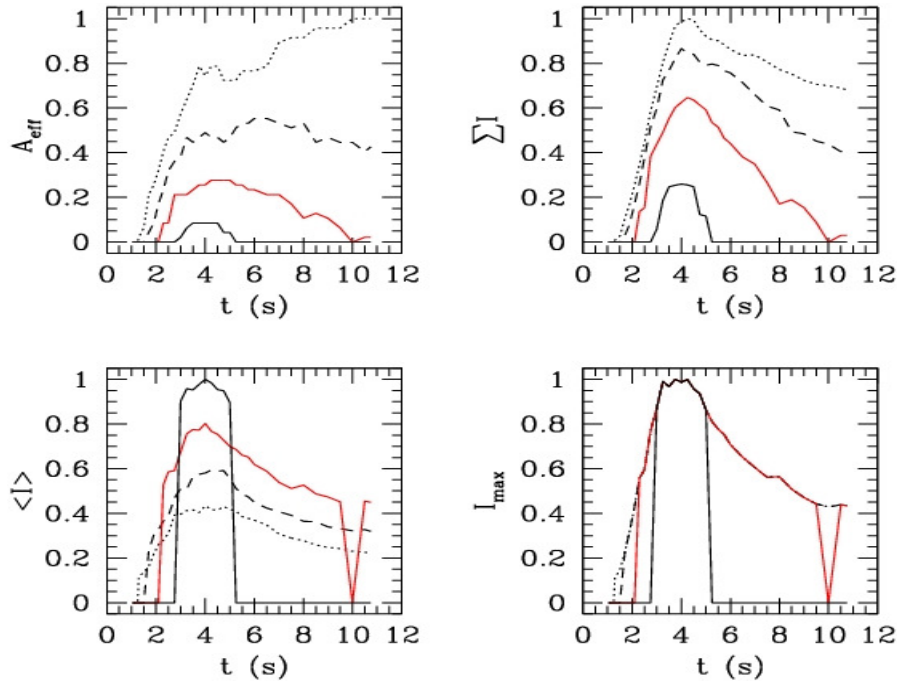


Figure 6: From left to right and top to bottom: time evolution of the effective area (A_{eff}), summed intensities (ΣI), mean intensity ($\langle I \rangle$) and maximum intensity (I_{max}) of the decoy.

4. INFRARED DECOY MODEL IMPLEMENTATION

The final result of the synthetic imagery of the decoy is compared with the measured imagery in figure 7. Note that the simulated (left column) and real decoy images (right column) next to each other in figure 6 are not compared exactly at the same time after the launch.

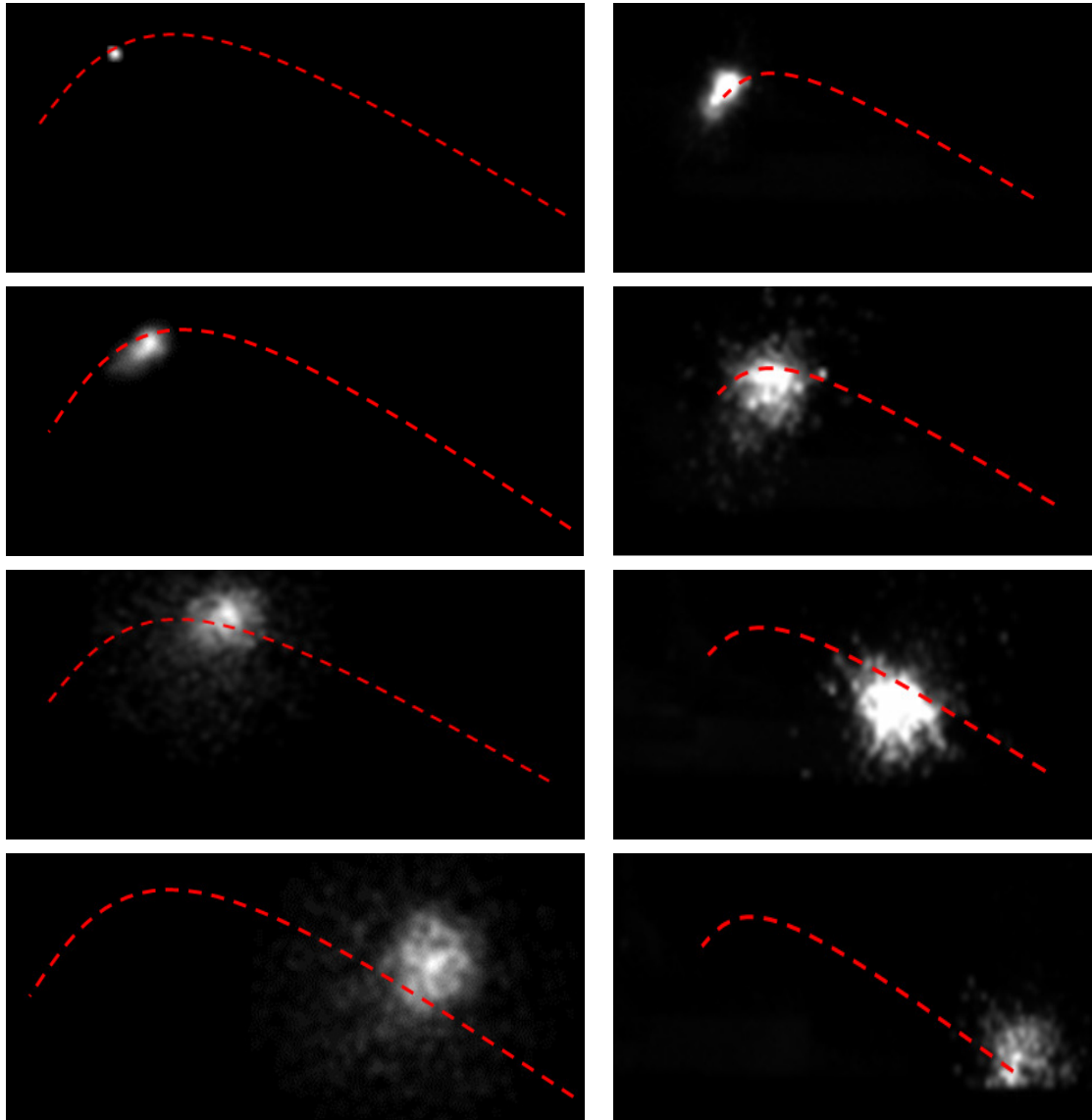


Figure 7: Synthetic imagery of the decoy (left column) is compared with the measured decoy imagery (right column)

5. SIMULATION OF DECOY EFFECTIVENESS

The simulation of decoys in the synthetic imagery is an enabler for decoy effectiveness studies. Figure 8 shows two simulated ship images in a synthetic background with simulated decoys. Note that the background contains not only clutter on the sea surface but also cloud clutter in the sky background. As in figure 3 the white rectangle indicates the track box of the seeker, which again grows with the target surface while the decoy and the ship overlap. The simulation now allows for variation in all parameters relevant for the performance of the decoy countermeasure such as aspect

angle, relative wind decoy, ship manoeuvres etc. Especially relevant for the development of decoy strategies are the positioning of the decoys and the number of decoys and the timing between the individual decoy launches.

The capability to insert decoys in image sequences can also be used to generate different decoy deployments in measured image sequences of ships without decoys. This is illustrated in figure 9 with imagery taken from the same sequence as used in figure 3, but now with the ship just before the decoy launch. One of the images shows an example of multiple decoy deployment. Special precautions need to be taken in the modelling when the decoys partially overlap.

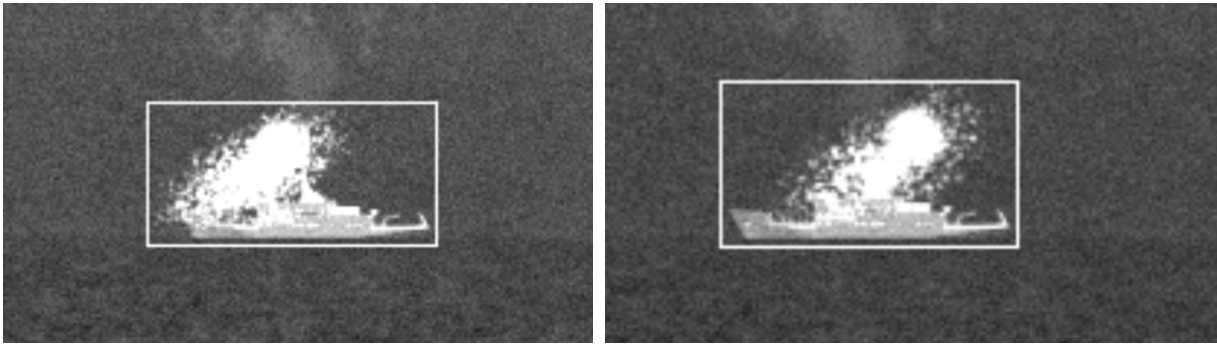


Figure 8: Simulated ship images in synthetic background and simulated decoys. The rectangle indicates the seeker track box.



Figure 9: Recorded imagery with synthetic decoys inserted: single decoy (left), multiple decoys (right).

6. SIMULATION OF SHIP SIGNATURE MANAGEMENT EFFECTS

As mentioned in section 2 the main goal of the trial was to evaluate the effects of signature management. As part of the signature management the ship had a hull cooling system on board. The goal of this hull cooling system was to cool the hull of the ship to a level which matches the background radiance level close to the horizon, thus minimising the contrast from the point of view of a missile tracker. Unfortunately however, the weather conditions during the trial did never create a situation where the solar load on the ship caused the hull temperature to rise to a level where the signature management system could really prove its value. The situation during the trial was such that the hull temperature was already close to the apparent background temperature even without hull cooling.

Now in order to demonstrate the effect of hull cooling on the survivability under high solar loading, we could use simulated imagery for these conditions. Basically the model suite calculates the temperature of all parts of the ship in thermal equilibrium. In order to simulate the active hull cooling, the model also enables us to replace the calculated temperature of some selected parts of the ship by the temperature which would be achieved by applying the hull cooling. The effect of replacing calculated temperature levels is better illustrated by actually increasing the temperature above the

calculated equilibrium temperature is shown in figure 10. The left panel shows the part of the ship in red where the temperature is replaced by a higher temperature. The middle panel shows the ship signature in equilibrium and the right panel shows the effect of an increased hull temperature.

Finally two simulated image sequences are shown figure 11 for a high and a low contrast situation. Running these sequences in the EWM seeker model allows evaluating the effectiveness of decoy deployment in these situations.



Figure 10: Effect of forced temperature changes in ship signature modelling. The left panel indicates the part of the ship in red where the temperature is replaced by a higher temperature. The middle panel shows the ship signature in equilibrium and the right panel shows the effect of an increased hull temperature.

7. SUMMARY AND CONCLUSIVE REMARKS

In this paper the extension of a toolset based on three TNO model suites EOSTAR, EOSM, and EWM with a detailed infrared decoy module has been discussed. The main reason for this extension was the requirement to be able to simulate decoy countermeasure deployment against infrared imaging seekers with detailed imagery, matching the spatial resolution of the seeker. The physical background of the flare model has been presented and the results are compared with measured data. Finally the application of this model suite to assess the effect of decoy deployment and signature management on the survivability of ships against infrared guided missiles has been demonstrated.

The results presented here have been analysed manually. For more extensive studies with multiple runs over multiple aspect angles for multiple scenarios, the batch mode capability of the EWM model will be used. Also within EWM tools are available for automatic analysis of the results in terms of “hit”, “no hit” or miss distance.

The next extension in the modelling will focus on modelling the infrared emission of the ship exhaust gas plume. Cooling the hot exhaust gases by mixing with cold air or by water injection is a signature management tool of interest. Analysis of plume cooling effectiveness requires a detailed plume model. The first step will be to develop the proper CFD (computational fluid dynamics) models to simulate the mixing of the resulting exhaust gases with the external air flow around the ship. Once the resulting flow field of the plume is determined, the next step is the calculation of the infrared emission from the distribution of temperature and radiating species in the plume. Finally this has to result in the insertion of an infrared image of the exhaust plume on the ship in the scene. This insertion will follow similar rules as the decoy insertion.

In conclusion: the successful extension of a toolset for countermeasure evaluation with a detailed infrared decoy module has been demonstrated.

8. ACKNOWLEDGEMENT

The authors would like to thank the Royal Netherlands Navy and the Defence Materiel Organisation for supporting this work. This work was sponsored by the Netherlands Ministry of Defence in the Maritime Countermeasure project under the Electronic Warfare research programme V1236.



Figure 11: Simulated image sequences for a high (left column) and a low (right column) contrast situation.

REFERENCES

1. H.M.A. Schleijsen, "Evaluation of infrared signature suppression of ships", in Targets and Backgrounds: Characterization and Representation II, W.R. Watkins, and D. Clement, editors, Proc. SPIE Vol. 2742, pages 245-254, Orlando (FL), USA, Apr. 1996.
2. H.M.A. Schleijsen, F.P. Neele, "Ship Exhaust Gas Plume Cooling", SPIE-2004 Orlando Targets and Backgrounds X: Characterisation and Representation, SPIE Vol. 5431, p 66, 2004.
3. F.P. Neele, and W. de Jong, "Prewetting systems as an IR signature control tool" in Targets and Backgrounds VIII: Characterization and Representation, W.R. Watkins, D. Clement, and W.R. Reynolds, editors, Proc. SPIE Vol. 4718, pages 156-163, Orlando (FL), USA, Apr. 2002
4. W. de Jong, S.P. van den Broek, and R. van der Nol, IR seeker simulator to evaluate IR decoy effectiveness in Targets and Backgrounds VIII: Characterization and Representation, W.R. Watkins, D. Clement, and W.R. Reynolds, editors, Proc. SPIE Vol. 4718, pages 164-172, Orlando (FL), USA, Apr. 2002
5. Wim de Jong, Frans A.M. Dam, Gerard J. Kunz, Ric. M.A. Schleijsen, "IR seeker simulator and IR scene generation to evaluate IR decoy Effectiveness", London 2004, Technologies for Optical Countermeasures, SPIE Vol 5614-11
6. Robin Schoemaker, Ric Schleijsen: "Evaluation Tools for the Effectiveness of Infrared Countermeasures and Signature Reduction for Ships", SPIE "infrared Imaging Systems: Design, Analysis, Modelling and Testing XXI, Vol 7662 paper 26. 2010.
7. Ric H. M. A. Schleijsen: "Toolset for evaluating infrared countermeasures and signature reduction for ships" (Invited Paper), SPIE Vol. 7836 paper 16, Technologies for Optical Countermeasures 2010.
8. F.A.M. Dam, W. de Jong, H.R. Mühren, "Naval ECM, a quantitative analysis", TNO Report TNO-DV 2008 A514, June 2009, Stg Confidentieel.
9. Marianne A. C. Degache, Alexander M. J. van Eijk, Dimitris Tsintikidis, Stephen M. Hammel, "EOSTAR Pro: a flexible extensive library to assess EO sensor performance" Optics in Atmospheric Propagation and Adaptive Systems, Toulouse 2010, SPIE Vol 7828-03.
10. A.L. Mieremet, W. de Jong, "EOSM validation using SAPPHIRE data", TNO report TNO-DV 2008 A253, June 2008, NATO restricted.
11. Michael Russell, The Chemistry of Fireworks, Royal Society of Chemistry, 1st edition, 2000
12. Zanetti, Air pollution modelling, Computational Mechanics Publications, 1990
13. Hanna, S.R., G.A. Briggs and R.P. Hosker, 1982: *Handbook on Atmospheric Diffusion*. DOE/TIC-11223, Department of Energy, 102 pp.;
14. Stamnes, K., Tsay, S.-C., Wiscombe, W., and Jayaweera, K.: Numerically stable algorithm for discrete-ordinate-method radiative transfer in multiple scattering and emitting layered media, Appl. Opt., 27, 2502-2509, 1988;
15. Stamnes, K., Tsay, S.-C., Wiscombe, W., and Laszlo, I.: DISORT, a general-purpose FORTRAN program for discrete-ordinate-method radiative transfer in scattering and emitting layered media: documentation and methodology, available from ftp://climate1.gsfc.nasa.gov/wiscombe/Multiple_Scatt/, 2000